Effects of infill patterns on part performances and energy consumption in acrylonitrile butadiene styrene fused filament fabrication via industrial-grade machine

Leopoldo De Bernardez[1] · Giampaolo Campana[2] · Mattia Mele[2] · Juan Sanguineti[1] · Cristian Sandre[1] · Sebastián Matías Mur[1]

Abstract

The industrial applications of Additive manufacturing technologies and systems are quickly increasing due to the high flexibility in the part design allowing for mass customisation and reduction of material usage. Besides the absence of manu-facturing tools permits a reduction of the time to market. Despite these relevant advantages, building time is generally high and it can typically determine significant energy consumption. Several studies investigate the effect of infill patterns on material mechanical properties to address the design of deposition patterns but these works do not take into consideration relevant aspects related to the manufacturing stage, such as the energy consumption, both the building paths and time. The choice of the infill pattern greatly affects the balance amongst part performances, energy and material consumption. On the other hand, a reduction of the deposited material can effectively reduce the building time and then the process energy. In the present paper, an index that quantifies this balance for a largely used Additive Manufacturing technology is introduced. For this purpose, an experimental investigation is carried out by monitoring the process energy during the manufacturing of specimens characterised by different infill patterns. Then, physical and mechanical properties are measured to compose the proposed index.

Keywords Fused filament fabrication · Fused deposition modelling · 3D printing · Infill pattern · Energy consumption · Tensile properties

1 Introduction

Additive manufacturing (AM), also known as 3D printing (3DP), is defined as "the process of joining materials to make parts from 3D model data, usually layer upon layer" [1]. This definition comprises a wide range of technologies that are rapidly transforming the manufacturing industry worldwide [2–4]. In fact, AM processes allow for surpassing several geometrical limitations of traditional technologies opening new opportunities in numerous industrial fields [5–7].

The global AM market was valued at 13.78 billion US dollars in 2020 and is expected to expand at a Compound Annual Grow Rate (CAGR) of 21% from 2021 to 2028 [8]. This tremendous expansion makes the research on the sustainability of AM a topic of pivotal importance [9]. Particularly, there is a body of research that has focused extensively on the assessment of the environmental impacts of 3DP [10]. Garcia et al. reviewed this research field showing that a

✉ Giampaolo Campana
giampaolo.campana@unibo.it

Leopoldo De Bernardez
ldb@itba.edu.ar

Mattia Mele
mattia.mele@unibo.it

Juan Sanguineti
jsanguinetti@itba.edu.ar

Cristian Sandre
scristian@itba.edu.ar

Sebastián Matías Mur
smur@itba.edu.ar

[1] Instituto Tecnológico de Buenos Aires (ITBA), Iguazú 341, C1437, Ciudad Autónoma de Buenos Aires, Argentina

[2] Department of Industrial Engineering (DIN), University of Bologna, Viale del Risorgimento 2, 40136 Bologna, Italy

major concern arises from the electrical consumption of AM technologies [11]. This can be explained considering that the 3DP-enabled design generally permits more efficient use of materials if compared to traditional processes [12, 13]. On the other hand, these technologies suffer from long process time, which determines an increase in machine usage and energy consumption [14, 15]. Therefore, there is a broad interest in the assessment of the energy consumption of AM processes [16, 17]. Liu et al. demonstrated that the energy efficiency of different AM processes can be significantly improved through a proper choice of process parameters without reducing product quality [18]. Nonetheless, there are still very limited studies on the relationships between process parameters and electrical consumption.

The 2021 annual report by Sculpteo revealed that the overwhelming majority of 3DP users deal with Fused Filament Fabrication (FFF) technology [19]. This process adopts a heated liquefier to melt a polymeric filament and deposit it layer-by-layer through a nozzle [20, 21]. Recently, this process has caused considerable interest within the industry due to the significant improvements in part quality and the increasing number of available materials [22, 23]. These results were achieved through careful optimisation of the parameters governing this process [24]. Particularly, the literature demonstrates that the mechanical properties of parts are deeply influenced by process parameters such as the nozzle temperature, layer height and extrusion rate [25–27]. These parameters also affect the quality of manufactured parts as far as dimensional accuracy is concerned [28–30]. Consequently, a number of experimental studies have been proposed to investigate the relations between process parameters and the characteristics of parts produced by FFF [31]. The results of this research can be used to optimise certain features of the manufactured products [32, 33]. This optimisation concerns not only the FFF process but also the successive operations [34–36].

Among process parameters, the deposition strategy has a crucial role in determining the part quality, dimensional accuracy, building time and mechanical properties [37, 38]. The deposition strategy is characterised by several parameters, such as the number of contour lines, the geometry of the infill and the distance between infill lines that is usually described through the infill density. All these parameters have a tremendous effect on the mechanical properties of the manufactured parts. Aloyaidi et al. demonstrated the effect of different infill patterns on the compression and impact strength of parts fabricated by Poly-Lactic Acid (PLA) [39]. A similar study was conducted by Yadav et al., who extended the investigation to different infill densities [40]. Wang et al. assessed the tensile strength of composite materials with hexagonal and triangular infill patterns printed at different densities [41]. The effect of combining different infill patterns on tensile properties was discussed in [42]. These studies highlight that the pattern geometry significantly affects the mechanical properties of the manufactured parts. Nonetheless, the behaviour of infill patterns is affected by their intersection with the contour lines of the specimens used for testing and is dependent on their orientation to the load. Consequently, the results presented in these papers are difficult to be reused when manufacturing more complex geometries. Overall, the results of the literature demonstrate that the mechanical resistance of manufactured parts increases with the infill density.

A common strategy for part filling is the use of a linear pattern, i.e., the deposition of parallel infill lines. Unlike previously discussed ones, this solution allows for nominal part densities up to 100%. It is worth underlining that the actual part density is always lower than 100% because parts suffer from porosities due to the intrinsic characteristics of the FFF process, as adequately explained in [43]. Porter et al. investigated the influence of differently oriented linear patterns (0°/90° and +45°/− 45°) on the flexural modulus of FFF parts [44]. Croccolo et al. experimentally characterised the tensile strength of Acrylonitrile Butadiene Styrene (ABS) M30 with a 100% dense linear pattern oriented at +45°/− 45°, and demonstrated the opportunity to achieve a reliable estimation of Young's modulus and Ultimate Tensile Strength (UTS) through analytical calculation [45]. These studies offer an in-depth insight into the effect of infill patterns on mechanical properties but do not consider other important aspects related to the manufacturing process such as the build time [46–48].

Peng highlighted the main sources of energy consumption in a desktop FFF printer [49, 50]. Nagarajan and Haapala compared the environmental impacts of Fused Deposition Modelling (FDM) of acrylonitrile styrene acrylate polymer filament to iron Direct Metal Laser Sintering (DMLS) by the Cumulative Exergy Demand (CExD). They found that the CExD of FDM is higher than DMLS [51].

A model to predict the energy consumption of FFF was proposed by Yi et al. [52]. Industrial machines usually have a different energy demand due to the heating of the building chamber. This power absorption was experimentally measured by Balogun et al. who highlighted the role of the time-temperature curve used for heating on the overall energy efficiency of the process [53]. Faludi et al. presented a complete Life Cycle Assessment (LCA) of an industrial FFF printer, namely a Stratasys Dimension 1200 BST. Their results highlight energy consumption as the main source of environmental impact. A significant amount of this impact is due to the energy necessary to heat the building chamber while the printer is in standby mode [54]. Overall, these studies deepen the understanding of FFF energy consumption but fail to correlate it with the most relevant process parameters. Specifically, no information is given on the role of infill patterns, which has been demonstrated to be crucial

to the duration and quality of this process. A recent systematic review of infill patterns in FFF was given by Jiang and Ma, who highlighted the need for an investigation of the relations between infill patterns and energy consumption as a possible area for future research [55].

The aim of this study is to investigate the effect of various linear infill patterns on mechanical performances, material and energy consumption of parts produced through an industrial FFF machine. This purpose is fulfilled through an experimental activity on a widely used material, namely ABS M30. The infill pattern and density are used as independent variables of the experiment. Based on the previously reviewed body of the literature, these parameters are expected to significantly affect the energy consumption and mechanical properties of the parts. Each factor is varied on three levels. A full factorial Design of the Experiment (DOE) is carried out, i.e., all the combinations of infill pattern and density are tested [56]. This approach was chosen to obtain a better insight into the non-linearities of relations between the infill parameters and the part properties. The energy consumed during the specimen manufacturing is monitored through a power meter. Then, part performances are acquired by tensile tests, and the observed results are also correlated to the infill toolpath to allow for the extension of the findings. Finally, a comprehensive index combining the mechanical properties, material and energy consumption is proposed and used for comparison purposes.

2 Material and methods

To identify a trade-off between the mechanical properties of parts, the amount of used material and the energy consumption, a set of specimens were printed for tensile tests that are characterised by different infill patterns and densities. The parts were designed by following the ASTM D638-14 type I standard [57]. The specimen is shown in (Fig. 1), which shows also the orientation of the machine coordinate system. The exterior surfaces of the specimens consisted of two contour lines, two top layers and two bottom layers oriented along the longitudinal axis.

A full factorial DOE was carried out using as factors the infill pattern and density. Linear infill patterns were considered. The orientation of the infill lines to the specimen longitudinal axis was varied on three levels, i.e., 0º, 90º and + 45º/− 45º. These infill strategies are shown in (Fig. 1) through a detailed view of the central part of the specimen. For each infill orientation, three different densities were investigated, namely 100, 90 and 80%.

Three repetitions of the experiment were carried out, leading to 27 final specimens. Each part was printed in a separate build job. The order of runs was randomised through the statistical software Minitab. The same software was used for the statistical elaboration of data at the end of the experiment.

The specimens were printed using a Fortus 250 3D printer by Stratasys Ltd. equipped with a T14 nozzle. This printer possesses a heated building chamber.

The printing conditions were modified within the ranges accepted by the GrabCAD Print slicer software and the Insight App. The materials and printing conditions are summarized in (Table 1).

The printer is plugged into the 220 V, 50 Hz, 1 phase line. The active energy required by the equipment in each run was measured and recorded by using an ElNet Energy and Powermeter having serial and TPC/IP interface ports allowing direct interface with a PC for data recording. The energy consumption was recorded during the whole printing

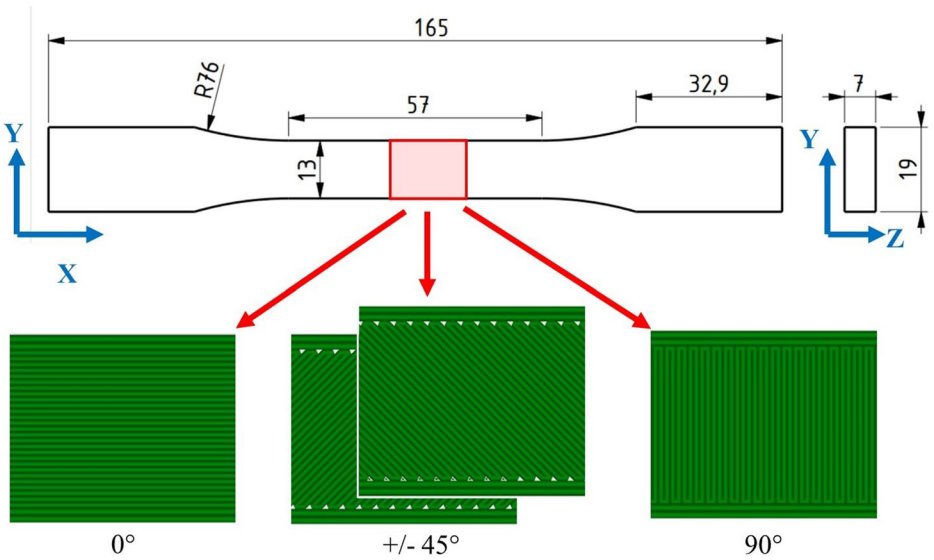

Fig. 1 Specimen geometry (dimensions in mm) and detailed view of the infill orientations investigated in this study

Table 1 Materials and printing conditions

Materials	
Model material	ABS P430
Support material	ABS SR30
Extruder	
Nozzle diameter (mm)	0.356
Nozzle temperature (ºC)	300
Build chamber	
Size (mm)	250 × 250 × 305
Temperature in standby mode (ºC)	72
Temperature while printing (ºC)	76
Insight parameters-support	
Support style	Basic
No. of base layers	5
Insight parameters-toolpath	
Part interior style	Sparse-low density
Part fill style	Multiple contours
No. of contours	2
No. of top and bottom solid layers	2
Contour line width (mm)	0.508
Top and bottom line width (mm)	0.508
Layer height (mm)	0.254
Raster width (mm)	0.406
Infill density (%)	100; 90; 80
Linear infill pattern with orientation (°)	0; 90; ± 45
Sparse raster air gap depending on infill (mm)	0; 0.056; 0.127

cycle, from standby mode to the end of the printing process. The data was then separated into different periods to distinguish the energy required for chamber heating from that used for printing. The latter includes the material fusion, the movements of the motors and the build chamber temperature maintenance.

The specimens were weighed at the end of the printing process and after removing the support layers.

The specimens were tested according to the ASTM D638-14 standard [58] with a universal testing machine Instron 3382 equipped with a long travel 2603–080 extensometer. The Instron machine including a specimen mounted for testing is shown in (Fig. 2). After mechanical tests, the fracture regions of the specimens were observed by means of a digital optical microscope Newvision G1200.

3 Results

The active energy measurements and printing times are presented in (Table 2) for different infill directions and densities. Since three replications were used for the experiment, the table reports all the individual measurements for each of the different infill orientations and densities to allow diverse elaborations by the reader.

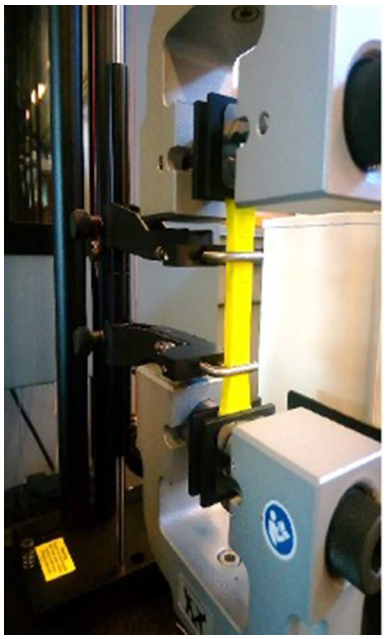

Fig. 2 Instron 3382 performing the tensile tests on a printed sample

The actual printing time of each build was measured by the operator using a digital stopwatch. It is worth noting that both the energy consumption and the production time decrease when the infill density diminishes. Being the infill density is the same, the maximum values of active energy and printing time are observed when the orientation of tracks is equal to 90°. Contrariwise, infill patterns at 0° show lower time and energy consumption if compared to other orientations with the same infill density.

The weight measurements are also shown in (Table 2). The difference between the total weight and that of the sample is due to the fact that the total weight includes the six layers of support deposited before starting to print the part. This support material is added by GrabCAD Print slicer to ease the detaching of parts from the building platform at the end of the process. The weight of the sample decreases accordingly with the infill density while the orientation of the infill pattern has no significant effects.

Figure 3 shows the stress–strain curves obtained during the tensile tests. The numerical values of UTS, elongation at break and Young's modulus are also reported in (Table 3). By observing (Fig. 3 and Table 3), it can be noticed that the UTS and Young's modulus change significantly with the infill orientation showing the lowest values for linear infill orientation equal to 90º and the highest ones for 0º. The tensile strength and modulus of parts decrease as the infill density decreases. The elongation at break does not show a clear trend.

Table 2 Measured values of active energy, printing time and weight for each infill direction

Orientation (°)	0			±45			90		
Infill (%)	80	90	100	80	90	100	80	90	100
Active energy (Wh)	336	385	418	485	515	551	493	536	579
	358	373	392	446	512	536	500	549	614
	320	378	384	448	516	553	516	548	574
Printing time (min)	37.1	40.0	42.6	51.7	56.5	61.6	55.9	61.6	66.5
	37.1	39.9	442.5	51.7	56.5	61.6	55.9	61.7	67.5
	37.1	40.0	42.6	51.7	56.5	61.6	55.9	61.7	67.5
Total weight (g)	17.37	18.53	20.55	17.35	19.00	20.56	17.38	18.76	20.63
	17.34	18.76	20.43	17.29	18.99	20.64	17.42	19.04	20.65
	17.44	18.63	20.47	17.45	18.87	20.65	17.49	19.05	20.66
Specimen weight (g)	15.30	16.45	18.47	15.28	16.94	18.49	15.36	16.69	18.57
	15.23	16.74	18.34	15.21	16.95	18.57	15.35	16.95	18.57
	15.36	16.58	18.40	15.37	16.80	18.59	15.43	169.5	18.59

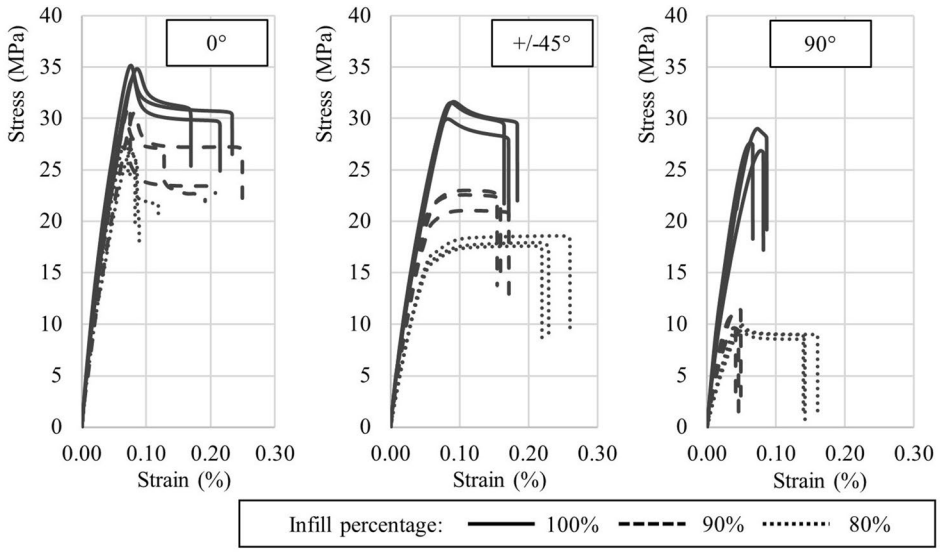

Fig. 3 Stress–strain curves obtained by tensile tests

Table 3 Measured values of Ultimate Tensile Strength, Elongation at break and Young's modulus

Orientation (°)	0			±45			90		
Infill (%)	80	90	100	80	90	100	80	90	100
Tensile strength (MPa)	27.6	30.6	34.0	17.9	21.0	30.0	9.9	9.7	29.0
	26.9	31.2	34.8	17.9	23.0	31.6	9.9	11.6	27.6
	27.9	30.5	35.2	18.5	22.6	31.5	9.4	10.7	26.9
Elongation at break (%)	8.25	19.14	21.45	16.94	17.15	17.10	16.02	4.55	8.65
	8.89	20.73	23.34	21.94	15.92	18.37	13.94	4.89	8.15
	12.40	24.90	16.94	26.00	15.40	16.45	14.19	4.13	6.62
Young's modulus (MPa)	697.3	657	712.2	391.4	534.5	629.8	297.3	445.3	720.8
	632.5	718.7	723.1	370.9	553.6	669.5	285.5	464.5	779.2
	691.3	700.7	795.9	381.0	526.0	615.0	280.8	504.2	684.0

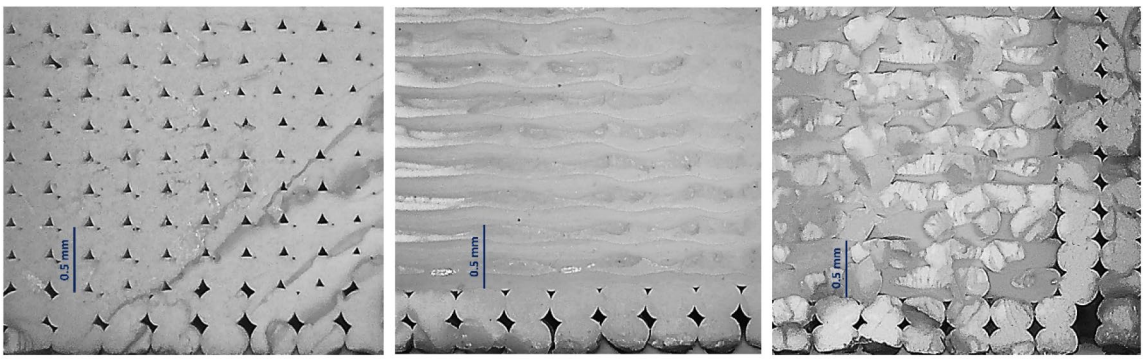

Fig. 4 Optical micrograph of a typical fracture surface after tensile tests. **a** 0º infill orientation and 100% infill density; **b** 90º infill orientation and 100% infill density; **c** + 45/− 45º infill orientation and 100% infill density

Examples of the fractured surfaces for the three different infill orientations are shown in (Fig. 4) for an infill density equal to 100%. It is possible to recognise the infill patterns and the exterior surface layers can be observed.

It is evident from (Fig. 4a) that the fracture surface is perpendicular to the raster orientation that is the same for both the inner and the contour lines. Despite the nominal infill density being 100%, it is possible to remark that empty regions between deposited lines are present. In (Fig. 4b), it is possible to remark that the fracture surface is parallel to the inner infill raster orientation and all the layers can be easily identified. The bottom layers are also clearly seen where the raster orientation is perpendicular to the fracture surface. For this orientation, it is still possible to identify empty regions between the deposited lines in the bottom layers. Figure 4c shows the fracture surface for + 45°/− 45º infill raster orientation where the layers cannot be easily identified by the optical micrograph. It is also possible to see that the fracture surface is perpendicular to the raster orientation of contour lines and bottom layers as in the previous cases.

4 Discussion

The experimental results in (Table 3) show that the UTS and Young's modulus of the specimens increase with the infill density. This finding is expected since the increase of infill density increases the amount of material withstanding the applied load. The relation between part weight and mechanical resistance shows different trends depending on the inner disposition of the deposited material (Fig. 5) and then the orientation of the raster pattern.

Particularly, it is observed that the UTS of parts with pattern 0° is almost linearly proportional to the mass of the part, i.e., to the percentage of infill. In this case, the deposited tracks are loaded along their axes. Therefore, a

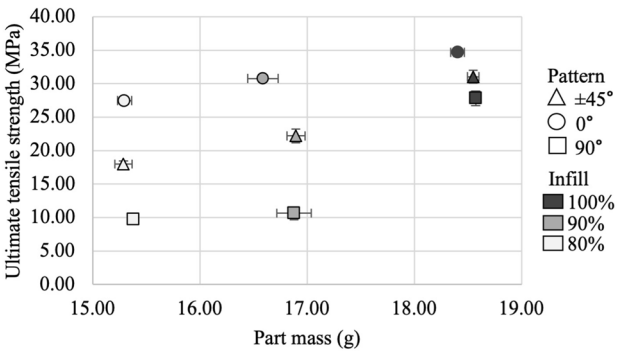

Fig. 5 Relation between part mass and Ultimate tensile strength for different infill orientations

change in the number of deposited tracks only determines a variation of the actual cross-section area of the specimen. Being the UTS estimated based on the nominal cross-section of the specimen (ISO/ASTM International, 2015), a linear relation can be observed between the calculated value and the measured mass. This consideration is supported by the observation of the fracture surface (Fig. 3a), which shows a transversal fracture of the deposited lines. A completely different trend is shown by specimens with infill at 90°. It is apparent that these parts show a sharp decrease of mechanical resistance moving from 100 to 90% infill (Fig. 5). This result can be explained by the fact that the raster lines are normal to the load direction. As a consequence, when the infill percentage is less than 100%, the material continuity along the load direction is broken, as schematically shown in (Fig. 6). The mechanical resistance to the applied load is thus primarily offered by the external contour of the part, the mass of which is only a small portion of the specimen. This interpretation also justifies the small differences observed in (Fig. 5) moving from 90 to 80% of the infill density. It can also be observed that, as far as 100% infill is concerned, this

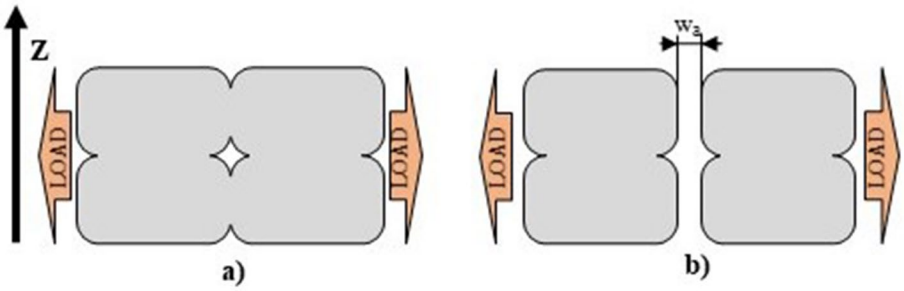

Fig. 6 Schematical representation of the sagittal section of specimens with infill at 90°. **a** Infill density 100%; **b** Infill density < 100%

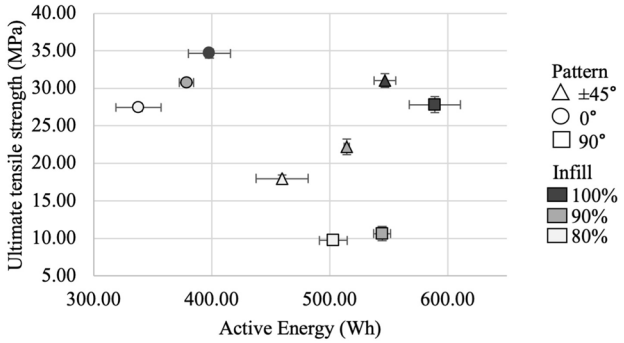

Fig. 7 Relation between energy consumption and tensile strength for patterns and infill densities

group of specimens shows lower mechanical strength than those oriented at 0°. This result can be explained because the resistance of the infill generated with linear paths oriented at 90° is determined by adhesive forces bonding adjacent raster lines that were deposited at the semi-molten state, which is considerably lower than the cohesive resistance of the full section withstanding the applied load [45].

In the case of infill + 45°/− 45°, the tensile strength is the result of a combination of adhesive and cohesive forces, as discussed by Croccolo et al. [45]. As shown in (Fig. 5), for each infill percentage, the UTS of these specimens is between those with infill at 90 and 0°. In this configuration each raster line is able to resist a portion of the applied force, namely the component along the axis line, also when $w_a > 0$ (see Fig. 6). The fracture mechanisms of the specimens are characterised by complex phenomena. This can also be seen in (Fig. 4c), where the deposited lines appear weaved in the fracture region. A detailed investigation of internal phenomena occurring in the material is out of the scope of this study.

In Fig. 7, the values of UTS are plotted as a function of the measured active energy for each infill strategy.

It is worth mentioning that the same mechanical properties can be achieved with significantly different energy consumptions depending on the deposition strategy. What stands out in this figure is that being the infill percentage equal, the 0° orientation allows for the achievement of the highest mechanical performances with the minimum energy consumption. The worst results are observed for orientation 90°.

While a justification for mechanical properties has been given above, further analysis of the system energy efficiency is necessary. This analysis is carried out under the assumption that the main contributions to the electrical consumption of the equipment are made by the axes motors, the extruder motor and the heating system that includes the heating system of the chamber and the melting system. In other words, the energy consumed by the LCD display and other electronic parts is assumed to be negligible. This seems to be a realistic assertion since the power requirement of these devices is usually far below the measured values. The effect that the deposition path variables have on the energy consumption is investigated using Analysis Of Variance (ANOVA). This technique compares the distributions of populations in a given dataset to determine to what extent the output values are influenced by the independent variables of the experiment [56]. The analysis considered the effects of four parameters of the infill pattern on measured active energy which may be influential, namely:

- The total length of movements in the XY plane (L_{xy});
- The number of movements in the XY plane (n_{xy});
- The percentage of movements in the XY plane carried out by using only one motor, i.e., parallelly to the *X* or the *Y*-axis, (p_{1m});
- The number of movements along the *Z*-axis (n_z).

The total length of movements in the XY plane L_{xy} is expected to govern the building time. Besides, the number of movements n_{xy} is considered since each movement requires a change of direction, which may result in additional printing time and energy. Whilst in general two motors are used for moving the extruder in the XY plane, movements parallel to the *X* or *Y*-axis require only one stepper motor. To understand if this implies a saving on the total energy consumption, the percentage of movements parallel to these axes p_{1m} is included in the analysis. The movements along the *Z*-axis are carried out by the platform, the drives of which differ from those of the extruders. The number of movements along the *Z*-axis n_z is included to assess their influence on

the overall energy consumption. All the parameter values were calculated from the GrabCAD Print slicer and the Insight App code output.

The ANOVA was carried out by means of the statistical software Minitab. The confidence level adopted in the analysis was equal to 95%. Table 4 summarises the results of the ANOVA. The significance of the investigated values is also graphically shown in (Fig. 8), which displays the Pareto chart of standardised effects. This chart provides a dimensionless representation of the magnitude and importance of effects aiding to understand the relative influence of each input variable [56].

Figure 8 shows that the total length (L_{xy}) and the number of paths (n_{xy}) exceed the critical standard value, which is represented by a vertical dashed line in the Pareto chart. That is to say that the influence of these parameters on energy consumption is statistically significant. The same result can also be seen in (Table 4), which shows that the p-value of these factors is less than 0.05 [56]. Conversely, the number of movements carried out using only one motor does not appear to significantly affect the output. In other words, the influence of the change in electricity consumption due to the number of motors used for moving in the plane is negligible. Analogously, no statistical influence of the parameter n_z is observed, i.e., the movements along the Z-axis seem irrelevant to the energy consumption. It must be stressed that these results are obtained from a limited number of experiments. Particularly, only one geometry printed in different conditions has been investigated. Therefore, further research is necessary to generalise these findings.

The results of ANOVA allow for concluding that L_{xy} and n_{xy} are the only variables affecting energy consumption. Interestingly, these factors are also the most relevant to the printing time (t_b). In fact, expressing L_{xy} in mm and t_b in seconds, the building time can be estimated through Eq. 1. This equation has an adjusted coefficient of determination R^2 equal to 99.92%, which shows the high accuracy of the regression [56].

$$t_b = 9.234 \times 10^2 + L_{xy}8.839 \times 10^{-3} + n_{xy}8.887 \times 10^{-2} \quad (1)$$

These results suggest that the effect of the infill strategy on energy consumption is mainly related to the differences in the time needed to complete the printing process. This conclusion is also supported by (Fig. 9), in which the measured active energy values are plotted as a function of the actual building time. Looking at (Fig. 9), it is apparent that the energy consumption is linearly proportional to the building time. In greater detail, the plotted data can be interpolated through a line with a coefficient of determination R^2 equal to 99.44%.

A possible explanation for this finding is that the heating of the build chamber accounts for most of the energy consumption of the process. To validate this hypothesis, an estimation of the electrical power needed to maintain the build chamber temperature was made by measuring the energy consumption during the standby mode of the printer. In this mode, the motors are not moving but the chamber is kept heated at 72 ºC. During the printing stage, the chamber temperature rises to 76 ºC (for ABS). Thus an evaluation of the energy consumption for heating the chamber during printing can be calculated starting from mentioned measurements in the standby mode by applying a correction for the difference

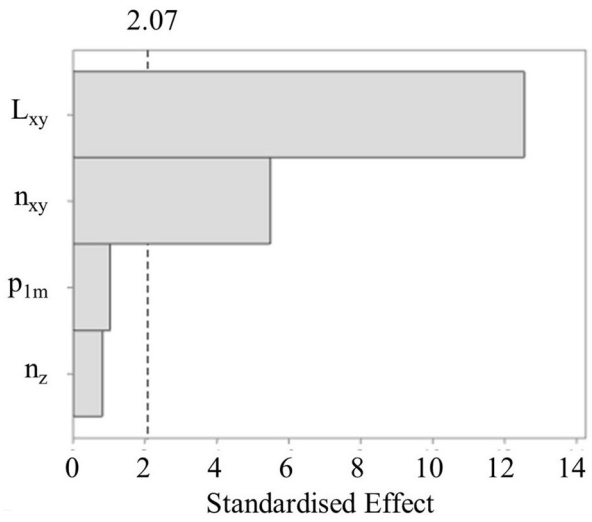

Fig. 8 Pareto chart of standardised effects of toolpath parameters on active energy

Table 4 ANOVA of measured active energy versus toolpath parameters

Source	Degrees of freedom	F-value	P-value
L_{xy}	1	30.03	0.000
n_{xy}	1	157.34	0.000
p_{1m}	1	0.67	0.420
n_z	1	1.04	0.319

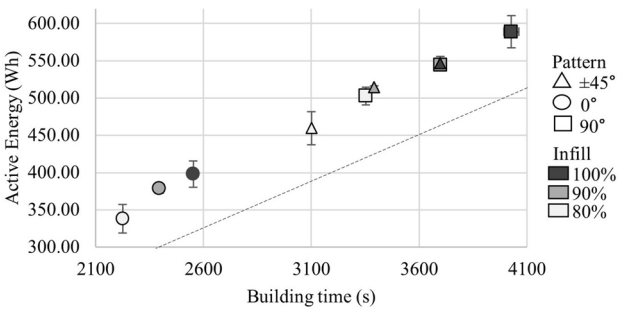

Fig. 9 Building time versus active energy consumption

between the temperature kept in the standby mode and in the printing mode. The calculated value of the average heating power was 451.3 W. The dashed line in (Fig. 9) represents the energy consumption associated with the need for the heated chamber. It is observed that the line runs approximately parallel to the measured active energy values. This supports the hypothesis that, in the scope of the investigated geometries, the time for which the building chamber is maintained at a high temperature is the main influential variable on the energy consumption of the process.

The error bars in (Fig. 9) show that the printing time is consistently repeatable, while some of the active energy values vary significantly around the average value. This result can also be observed by looking at the dispersion of data in Table 2. These differences can be in part due to the variability in the initial chamber heating phase. This phase is included in the active energy value since the measurement starts when the print job is launched. Nevertheless, the time span between two consecutive jobs can significantly affect the temperature from which the chamber heating starts and, consequently, the amount of energy necessary to reach the building temperature. This time interval between print jobs has not been controlled in this experiment, therefore its effect may be responsible for the observed variation of measured data. This is confirmed by the results presented in (Fig. 9), which demonstrate the prominent role of the heating phase in determining the total energy consumption. Based on these results, an important practical recommendation is to plan the FFF production so as to reduce as much as possible the inactive time between consecutive jobs, since this can strongly influence the energetic efficiency of the process. The active power consumed during the standby mode also suggests that this phase should be limited as it is responsible for substantial impacts. This argument is consistent with the findings of (Faludi et al. 2015). Nevertheless, the producer of the printer currently recommends maintaining the equipment in standby mode when inactive to ensure the best printing quality and extend the lifespan of the machine. Arguably, this need should be surpassed in future machine designs to improve the sustainability of the process.

As discussed in the introduction, several studies have been published examining the environmental, economic and social impacts of AM [59]. This research interest led to the definition of a considerable number of indices quantifying the process sustainability [60]. These indicators can be used to provide a detailed description of the manufacturing impacts but do not allow a univocal determination of the most convenient among different solutions. In particular, they cannot be applied to select the less impactful infill pattern in FFF. Therefore, a new dimensionless Sustainability Index (SI) is proposed here to make this decision-making activity easier for designers.

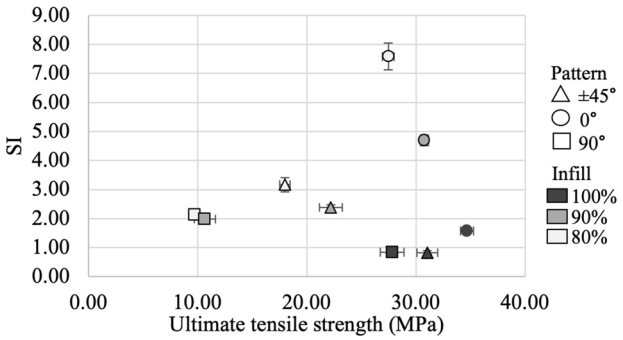

Fig. 10 Relation between sustainability index and tensile strength for different patterns and infill densities

The sustainability of AM processes is known to depend mainly on the equipment, material and energy consumption [14, 61, 62]. Whilst equipment is assumed to be fixed, both material and energy consumption are strongly affected by the infill strategy, as discussed above. It has been shown by previous studies that the material has a considerable effect on the overall impacts of FFF [63, 64]. The material saving achieved through the infill strategy is considered in the proposed SI through the difference (ΔV) between the nominal volume of the part (V_N) and the volume of the deposited material. The latter is obtained from the actual printed mass of the part, M, divided by the nominal material density, ρ. The SI is directly proportional to the material saving (ΔV, measured in m^3).

The importance to reduce the energy consumption of AM processes has been exhaustively discussed in the literature [18, 61, 65]. Therefore, the SI is inversely proportional to the active energy (E_A, measured in J).

The infill pattern must also be chosen considering the mechanical properties of manufactured parts. Particularly, one of the primary objectives is to maximise the stiffness of manufactured parts [39, 66]. Accordingly, the SI is directly proportional to Young's modulus (E, measured in MPa).

Based on these considerations, the proposed adimensional SI is calculated according to Eq. 2:

$$SI = \frac{E}{E_A} \times \Delta V = \frac{E}{E_A} \times \left(V_N - \frac{M}{\rho} \right) \quad (2)$$

By observing Eq. (2), it can be seen that the index increases if the stiffness of the piece increases but decreases if energy and material consumption increases. This is in line with the considerations on the impacts of the FFF process exposed above.

In the present study, the nominal volume V_N is equal to 18.368 cm^3, the mass of each printed part is measured (see Tab. 2), and the nominal material density is $\rho = 1.05$ g/cm^3, as indicated by the producer [67].

Figure 10 shows the SI values as a function of the UTS of the part.

As can be observed, the highest SI values are obtained when the orientation of the infill is 0º and the lowest values for an orientation equal to 90º. This result is mainly driven by the highest mechanical properties and the lower building time of those specimens with infill 0°.

An interesting result can be observed when the orientation is 0º because the index increases when the infill density decreases, although this means lower values of the mechanical resistance of the piece. The same trend is observed for the other orientations, even if a different slope of the curve is observed. This can be once again explained by considering the different relations between mechanical resistance and building time outlined in previous paragraphs. The SI could be used in a real design scenario to select the most sustainable solution among those satisfying the mechanical requirements of the application. Particularly, the tensile strength imposed by the design can be represented as a vertical line in (Fig. 10). Among the solutions lying on the right of this line, the one with the highest value of SI should be preferred. This approach allows for easily identifying the solution which minimises the material and energy consumption while achieving design requirements in terms of mechanical resistance. From these results, it seems possible to find a certain trade-off that could improve the sustainability of the production by using less material and energy if it is acceptable in terms of the mechanical properties of the printed part.

5 Conclusion

The experimental findings of this study pointed out that the production of parts through professional FFF equipment suffers from relevant energy consumption and emphasised the need for a decision-making approach to reduce its impact. For this purpose, an experimental campaign was carried out by printing several samples with different strategies. The energy consumption and mechanical performance were measured.

It was found that most of the electrical power is spent to heat the build chamber. In addition, a conspicuous waste of energy was observed when the machine is not printing, i.e., in standby mode, because the chamber is maintained at high temperatures. As a result, this study suggests the need for new technical solutions able to reduce the use of electricity when not working. The presented evidence also indicates that careful planning of jobs is crucial to limit the impacts of the process.

The results obtained from tensile tests carried out in this study confirm that the mechanical properties of parts produced through FFF largely depend on the infill strategies adopted for hatching, but in particular, a prominent role of the infill orientation was observed. It was also found that the hatching strategy governs the building time and, as a consequence, the heating energy.

Statistical analysis was carried out to relate the hatching path to the building time. The results demonstrated that the print duration is closely related to the total length of the hatching path and the number of deposited lines. This finding is of great relevance to guiding the selection of infill strategy toward a reduction of energy consumption. This result can be used to extend to more complex geometries the conclusions drawn in this study. As demonstrated by the experiments, this is crucial when industrial machines with heated chambers are used for printing.

The weight measurements performed on specimens demonstrated that the infill strategy has a considerable influence also on the amount of deposited material, which was demonstrated by previous literature to be crucial to FFF sustainability. Furthermore, the results of this study show that the total amount of material is largely influenced by the presence of support layers. This influence becomes even more relevant in the case of small parts with complex geometry.

Overall, the findings of this study highlight the pivotal role of the infill strategy as far as mechanical properties of parts, energy and material consumption are concerned. The presented results suggest that these aspects must be carefully considered when choosing the infill strategy, part orientation and design. To support this decision-making process, a novel dimensionless index that comprises information on material and energy consumption, and mechanical properties was proposed. It was found that this index allows for easy comparison among different alternative solutions. Particularly, the application to the investigated specimens demonstrated that hatching orientation at 0° is preferable due to higher mechanical properties and lower building time. The index can be used to guide the FFF planning toward more sustainable use of resources.

The findings of this research are significant in at least two main aspects. First, practical recommendations for users and developers of FFF were obtained based on more in-depth insight into energy and material consumption, and mechanical performances. Second, the novel index proposed in this study allows for easily comparing different solutions considering both mechanical and environmental performances.

Acknowledgements The authors would like to thank the MIUR (Italian Ministry of University and Research) for funding support and the ITBA for laboratory facilities.

Data availability Please, contact the authors if you are interested in the raw data required to reproduce these findings that are available to download.

Declarations

Conflict of interest The authors declare that they have no known competing financial interests or personal relationships that could have appeared to influence the work reported in this paper.

References

1. ISO/ASTM International (2015) ISO/ASTM 52900 - Additive manufacturing - General principles - Fundamentals and vocabulary
2. Dilberoglu UM, Gharehpapagh B, Yaman U, Dolen M (2017) The role of additive manufacturing in the era of industry 4.0. Procedia Manuf 11:545–554. https://doi.org/10.1016/j.promfg.2017.07.148
3. Gao W, Zhang Y, Ramanujan D et al (2015) The status, challenges, and future of additive manufacturing in engineering. CAD Comput Aided Des 69:65–89. https://doi.org/10.1016/j.cad.2015.04.001
4. Ngo TD, Kashani A, Imbalzano G et al (2018) Additive manufacturing (3D printing): a review of materials, methods, applications and challenges. Compos Part B Eng 143:172–196. https://doi.org/10.1016/j.compositesb.2018.02.012
5. Ali MH, Batai S, Sarbassov D (2019) 3D printing: a critical review of current development and future prospects. Rapid Prototyp J 25:1108–1126. https://doi.org/10.1108/RPJ-11-2018-0293
6. Doubrovski Z, Verlinden JC, Geraedts JMP (2011) Optimal design for additive manufacturing: Opportunities and challenges. In: Proceedings of the ASME Design Engineering Technical Conference. 635–646
7. Mehrpouya M, Dehghanghadikolaei A, Fotovvati B, et al (2019) The Potential of Additive Manufacturing in the Smart Factory Industrial 4.0: A Review. Appl Sci 34
8. MarketResearch.com (2022) 3D printing market size, share & trends analysis report by component (Hardware, Software, Services), by printer type, by technology, by software, by application, by vertical, by region, and segment forecasts 2022–2030. Accessed 17 June 2022
9. Ford S, Despeisse M (2016) Additive manufacturing and sustainability: an exploratory study of the advantages and challenges. J Clean Prod 137:1573–1587. https://doi.org/10.1016/j.jclepro.2016.04.150
10. Saade MRM, Yahia A, Amor B (2020) How has LCA been applied to 3D printing? A systematic literature review and recommendations for future studies. J Clean Prod 244:118803. https://doi.org/10.1016/j.jclepro.2019.118803
11. Garcia FL, da Moris VAS, Nunes AO, Silva DAL (2018) Environmental performance of additive manufacturing process – an overview. Rapid Prototyp J 24:1166–1177. https://doi.org/10.1108/RPJ-05-2017-0108
12. Huang R, Riddle M, Graziano D et al (2016) Energy and emissions saving potential of additive manufacturing: the case of lightweight aircraft components. J Clean Prod 135:1559–1570. https://doi.org/10.1016/j.jclepro.2015.04.109
13. Tang Y, Mak K, Zhao YF (2016) A framework to reduce product environmental impact through design optimization for additive manufacturing. J Clean Prod 137:1560–1572. https://doi.org/10.1016/j.jclepro.2016.06.037
14. Le Bourhis F, Kerbrat O, Hascoet J-Y, Mognol P (2013) Sustainable manufacturing: evaluation and modeling of environmental impacts in additive manufacturing. Int J Adv Manuf Technol 69:1927–1939. https://doi.org/10.1007/s00170-013-5151-2
15. Lindemann C, Jahnke U, Moi M, Koch R (2012) Analyzing product lifecycle costs for a better understanding of cost drivers in additive manufacturing. In: 23th annual international solid freeform fabrication symposium–an additive manufacturing conference. Austin Texas USA 6th-8th August 177–188
16. Baumers M, Tuck C, Bourell DL et al (2011) Sustainability of additive manufacturing: measuring the energy consumption of the laser sintering process. Proc Inst Mech Eng Part B J Eng Manuf 225:2228–2239. https://doi.org/10.1177/0954405411406044
17. Fruggiero F, Lambiase A, Bonito R, Fera M (2019) The load of sustainability for additive manufacturing processes. Procedia Manuf 41:375–382. https://doi.org/10.1016/j.promfg.2019.09.022
18. Liu Z, Jiang Q, Ning F et al (2018) Investigation of energy requirements and environmental performance for additive manufacturing processes. Sustain. https://doi.org/10.3390/su10103606
19. Sculpteo.com (2021) The state of 3D printing, 2021 Edition. Accessed 17 June 2022
20. Turner BN, Strong R, Gold SA (2014) A review of melt extrusion additive manufacturing processes: I. Process design and modeling. Rapid Prototyp J 20:192–204
21. Turner BN, Gold SA (2015) A review of melt extrusion additive manufacturing processes: II. Materials, dimensional accuracy, and surface roughness. Rapid Prototyp J 21:250–261. https://doi.org/10.1108/RPJ-02-2013-0017
22. Ciotti M, Campana G, Mele M (2021) A review of the accuracy of thermoplastic polymeric parts fabricated by additive manufacturing. Rapid Prototyp J ahead-of-p: https://doi.org/10.1108/RPJ-11-2020-0295
23. Singh S, Singh G, Prakash C, Ramakrishna S (2020) Current status and future directions of fused filament fabrication. J Manuf Process 55:288–306. https://doi.org/10.1016/j.jmapro.2020.04.049
24. Mohamed OA, Masood SH, Bhowmik JL (2015) Optimization of fused deposition modeling process parameters: a review of current research and future prospects. Adv Manuf 3:42–53. https://doi.org/10.1007/s40436-014-0097-7
25. Butt J, Bhaskar R, Mohaghegh V (2021) Investigating the effects of extrusion temperatures and material extrusion rates on FFF-printed thermoplastics. Int J Adv Manuf Technol 117:2679–2699. https://doi.org/10.1007/s00170-021-07850-5
26. Belarbi YE, Guessasma S, Belhabib S et al (2021) Effect of printing parameters on mechanical behaviour of pla-flax printed structures by fused deposition modelling. Materials (Basel) 14:1–17. https://doi.org/10.3390/ma14195883
27. Kechagias JD, Vidakis N, Petousis M (2021) Parameter effects and process modeling of FFF-TPU mechanical response. Mater Manuf Process. https://doi.org/10.1080/10426914.2021.2001523
28. Hanon MM, Zsidai L, Ma Q (2021) Accuracy investigation of 3D printed PLA with various process parameters and different colors. Mater Today Proc 42:3089–3096. https://doi.org/10.1016/j.matpr.2020.12.1246
29. Chaidas D, Kechagias JD (2021) An investigation of PLA/W parts quality fabricated by FFF. Mater Manuf Process 00:1–9. https://doi.org/10.1080/10426914.2021.1944193
30. Galetto M, Verna E, Genta G (2021) Effect of process parameters on parts quality and process efficiency of fused deposition modeling. Comput Ind Eng 156:107238. https://doi.org/10.1016/j.cie.2021.107238
31. Syrlybayev D, Zharylkassyn B, Seisekulova A et al (2021) Optimisation of strength properties of FDM printed parts—A critical review. Polymers (Basel). https://doi.org/10.3390/polym13101587
32. Schneidler J, Berry C, Barari A (2021) Improving 3D printing geometric accuracy using design of experiments on process parameters in fused filament fabrication (FFF). 14th IEEE Int

Conf Ind Appl INDUSCON. https://doi.org/10.1109/INDUSCON51756.2021.9529615
33. Shakeri Z, Benfriha K, Shirinbayan M et al (2021) Mathematical modeling and optimization of fused filament fabrication (Fff) process parameters for shape deviation control of polyamide 6 using taguchi method. Polymers (Basel). https://doi.org/10.3390/polym13213697
34. Castro-Casado D (2021) Chemical treatments to enhance surface quality of FFF manufactured parts: a systematic review. Prog Addit Manuf 6:307–319. https://doi.org/10.1007/s40964-020-00163-1
35. Kechagias JD, Ninikas K, Petousis M, Vidakis N (2021) Laser cutting of 3D printed acrylonitrile butadiene styrene plates for dimensional and surface roughness optimization. Int J Adv Manuf Technol. https://doi.org/10.1007/s00170-021-08350-2
36. Nagendra J, Srinath MK, Sujeeth S et al (2021) Optimization of process parameters and evaluation of surface roughness for 3D printed nylon-aramid composite. Mater Today Proc 44:674–682. https://doi.org/10.1016/j.matpr.2020.10.609
37. Jiang J, Ma Y (2020) Path planning strategies to optimize accuracy, quality, build time and material use in additive manufacturing: a review. Micromachines. https://doi.org/10.3390/MI11070633
38. Jayakumar N, Senthilkumar G, Pradeep A (2021) Effect of printing parameters of 3D printed PLA Parts on mechanical properties. J Eng Res. https://doi.org/10.36909/jer.icmmm.15697
39. Aloyaydi B, Sivasankaran S, Mustafa A (2020) Investigation of infill-patterns on mechanical response of 3D printed poly-lactic-acid. Polym Test 87:106557. https://doi.org/10.1016/j.polymertesting.2020.106557
40. Yadav P, Sahai A, Sharma RS (2020) Strength and surface characteristics of FDM-based 3D printed PLA parts for multiple infill design patterns. J Inst Eng Ser C. https://doi.org/10.1007/s40032-020-00625-z
41. Wang K, Xie X, Wang J et al (2020) Effects of infill characteristics and strain rate on the deformation and failure properties of additively manufactured polyamide-based composite structures. Results Phys 18:103346. https://doi.org/10.1016/j.rinp.2020.103346
42. Dezaki ML, Mohd AM, K. A. (2020) The effects of combined infill patterns on mechanical properties in fdm process. Polymers (Basel) 12:1–20. https://doi.org/10.3390/polym12122792
43. Al-Maharma AY, Patil SP, Markert B (2020) Effects of porosityon the mechanical properties of additively manufactured components: a critical review. Mater Res Express 7(2020):122001. https://doi.org/10.1088/2053-1591/abcc5d
44. Porter JH, Cain TM, Fox SL, Harvey PS (2019) Influence of infill properties on flexural rigidity of 3D-printed structural members. Virtual Phys Prototyp 14:148–159. https://doi.org/10.1080/17452759.2018.1537064
45. Croccolo D, De Agostinis M, Olmi G (2013) Experimental characterization and analytical modelling of the mechanical behaviour of fused deposition processed parts made of ABS-M30. Comput Mater Sci 79:506–518. https://doi.org/10.1016/j.commatsci.2013.06.041
46. Ganganath N, Cheng CT, Fok KY, Tse CK (2016) Trajectory planning for 3D printing: A revisit to traveling salesman problem. Proc-2016 2nd Int Conf Control Autom Robot ICCAR. https://doi.org/10.1109/ICCAR.2016.7486742
47. Jin Y, He Y, Fu G et al (2017) A non-retraction path planning approach for extrusion-based additive manufacturing. Robot Comput Integr Manuf 48:132–144. https://doi.org/10.1016/j.rcim.2017.03.008
48. Volpato N, Galvão LC, Nunes LF et al (2020) Combining heuristics for tool-path optimisation in material extrusion additive manufacturing. J Oper Res Soc 71:867–877. https://doi.org/10.1080/01605682.2019.1590135
49. Peng T (2016) Analysis of energy utilization in 3D printing processes. Procedia CIRP 40:62–67. https://doi.org/10.1016/j.procir.2016.01.055
50. Peng T (2017) Energy modelling for FDM 3D printing from a life cycle perspective. Int J Manuf Res 11:1. https://doi.org/10.1504/ijmr.2017.10003722
51. Nagarajan HPN, Haapala KR (2018) Characterizing the influence of resource-energy-exergy factors on the environmental performance of additive manufacturing systems. J Manuf Syst 48:87–96. https://doi.org/10.1016/j.jmsy.2018.06.005
52. Yi L, Ravani B, Aurich JC (2020) Development and validation of an energy simulation for a desktop additive manufacturing system. Addit Manuf 32:101021. https://doi.org/10.1016/j.addma.2019.101021
53. Balogun VA, Kirkwood ND, Mativenga PT (2014) Direct electrical energy demand in fused deposition modelling. Procedia CIRP 15:38–43. https://doi.org/10.1016/j.procir.2014.06.029
54. Faludi J, Bayley C, Bhogal S, Iribarne M (2015) Comparing environmental impacts of additive manufacturing vs traditional machining via life-cycle assessment. Rapid Prototyp J 21:14–33. https://doi.org/10.1108/RPJ-07-2013-0067
55. Jiang J, Xu X, Stringer J (2019) Optimization of process planning for reducing material waste in extrusion based additive manufacturing. Robot Comput Integr Manuf 59:317–325. https://doi.org/10.1016/j.rcim.2019.05.007
56. Montgomery D C (2019) Design and analysis of experiments. 10th Edition. Wiley. **ISBN: 978-1-119-63542-0**
57. Laureto JJ, Pearce JM (2018) Anisotropic mechanical property variance between ASTM D638–14 type i and type iv fused filament fabricated specimens. Polym Test 68:294–301. https://doi.org/10.1016/j.polymertesting.2018.04.029
58. García-Domínguez A, Claver J, Camacho AM, Sebastián MA (2020) Considerations on the applicability of test methods for mechanical characterization of materials manufactured by FDM. Materials (Basel) 13:28. https://doi.org/10.3390/ma13010028
59. Khalid M, Peng Q (2021) Sustainability and environmental impact of additive manufacturing: a literature review. Comput Aided Des 18:1210–1232. https://doi.org/10.14733/cadaps.2021.1210-1232
60. Taddese G, Durieux S, Duc E (2020) Sustainability performance indicators for additive manufacturing: a literature review based on product life cycle studies. Int J Adv Manuf Technol 107:3109–3134. https://doi.org/10.1007/s00170-020-05249-2
61. Mele M, Campana G, Fumelli G (2021) Environmental impact assessment of arburg plastic freeforming additive manufacturing. Sustain Prod Consum 28:405–418. https://doi.org/10.1016/j.spc.2021.06.012
62. Faludi J, Baumers M, Maskery I, Hague R (2017) Environmental impacts of selective laser melting: do printer, powder, or power dominate? J Ind Ecol 21:S144–S156. https://doi.org/10.1111/jiec.12528
63. Faludi J, Van Sice CM, Shi Y et al (2019) Novel materials can radically improve whole-system environmental impacts of additive manufacturing. J Clean Prod 212:1580–1590. https://doi.org/10.1016/j.jclepro.2018.12.017
64. Campana G, Mele M, Ciotti M, Rocchi A (2021) Environmental impacts of self-replicating three-dimensional printers. Sustain Mater Technol 30:e00335. https://doi.org/10.1016/j.susmat.2021.e00335

65. Peng T, Kellens K, Tang R et al (2018) Sustainability of additive manufacturing: An overview on its energy demand and environmental impact. Addit Manuf 21:694–704. https://doi.org/10.1016/j.addma.2018.04.022
66. Kwok TH, Li Y, Chen Y (2016) A structural topology design method based on principal stress line. CAD Comput Aided Des 80:19–31. https://doi.org/10.1016/j.cad.2016.07.005
67. Stratasys.com (2021) BS-M30 product data sheet. FDM thermoplastic filament. Accessed 17 June 2022